JOURNAL OF Applied Polymer SCIENCE

Special Issue: Microfiltration and Ultrafiltration Membrane Science and Technology

Guest Editors: Prof. Isabel C. Escobar (University of Toledo) and Prof. Bart Van der Bruggen (University of Leuven)

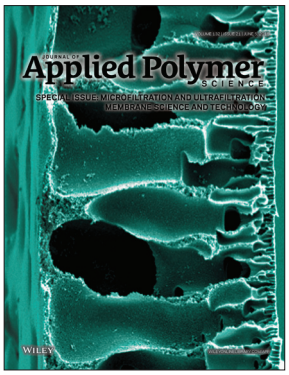

EDITORIAL

Microfiltration and Ultrafiltration Membrane Science and Technology
I. C. Escobar and B. Van der Bruggen, *J. Appl. Polym. Sci.* 2015, **DOI: 10.1002/app.42002**

REVIEWS

Nanoporous membranes generated from self-assembled block polymer precursors: *Quo Vadis*?
Y. Zhang, J. L. Sargent, B. W. Boudouris and W. A. Phillip, *J. Appl. Polym. Sci.* 2015, **DOI: 10.1002/app.41683**

Making polymeric membranes anti-fouling via "grafting from" polymerization of zwitterions
Q. Li, J. Imbrogno, G. Belfort and X.-L. Wang, *J. Appl. Polym. Sci.* 2015, **DOI: 10.1002/app.41781**

Fouling control on MF/ UF membranes: Effect of morphology, hydrophilicity and charge
R. Kumar and A. F. Ismail, *J. Appl. Polym. Sci.* 2015, **DOI: 10.1002/app.42042**

EMERGING MATERIALS AND FABRICATION

Preparation of a poly(phthalazine ether sulfone ketone) membrane with propanedioic acid as an additive and the prediction of its structure
P. Qin, A. Liu and C. Chen, *J. Appl. Polym. Sci.* 2015, **DOI: 10.1002/app.41621**

Preparation and characterization of MOF-PES ultrafiltration membranes
L. Zhai, G. Li, Y. Xu, M. Xiao, S. Wang and Y. Meng, *J. Appl. Polym. Sci.* 2015, **DOI: 10.1002/app.41663**

Tailoring of structures and permeation properties of asymmetric nanocomposite cellulose acetate/silver membranes
A. S. Figueiredo, M. G. Sánchez-Loredo, A. Maurício, M. F. C. Pereira, M. Minhalma and M. N. de Pinho, *J. Appl. Polym. Sci.* 2015, **DOI: 10.1002/app.41796**

LOW-FOULING POLYMERS

Low fouling polysulfone ultrafiltration membrane via click chemistry
Y. Xie, R. Tayouo and S. P. Nunes, *J. Appl. Polym. Sci.* 2015, **DOI: 10.1002/app.41549**

Elucidating membrane surface properties for preventing fouling of bioreactor membranes by surfactin
N. Behary, D. Lecouturier, A. Perwuelz and P. Dhulster, *J. Appl. Polym. Sci.* 2015, **DOI: 10.1002/app.41622**

PVC and PES-*g*-PEGMA blend membranes with improved ultrafiltration performance and fouling resistance
S. Jiang, J. Wang, J. Wu and Y. Chen, *J. Appl. Polym. Sci.* 2015, **DOI: 10.1002/app.41726**

Improved antifouling properties of TiO_2/PVDF nanocomposite membranes in UV coupled ultrafiltration
M. T. Moghadam, G. Lesage, T. Mohammadi, J.-P. Mericq, J. Mendret, M. Heran, C. Faur, S. Brosillon, M. Hemmati and F. Naeimpoor, *J. Appl. Polym. Sci.* 2015, **DOI: 10.1002/app.41731**

Development of functionalized doped carbon nanotube/polysulfone nanofiltration membranes for fouling control
P. Xie, Y. Li and J. Qiu, *J. Appl. Polym. Sci.* 2015, **DOI: 10.1002/app.41835**

JOURNAL OF Applied Polymer SCIENCE

Special Issue: Microfiltration and Ultrafiltration Membrane Science and Technology

Guest Editors: Prof. Isabel C. Escobar (University of Toledo) and
Prof. Bart Van der Bruggen (University of Leuven)

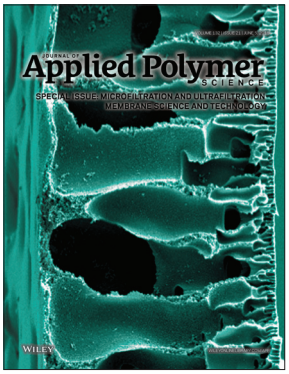

SURFACE MODIFICATION OF POLYMER MEMBRANES

Highly chlorine and oily fouling tolerant membrane surface modifications by *in situ* polymerization of dopamine and poly(ethylene glycol) diacrylate for water treatment
K. Yokwana, N. Gumbi, F. Adams, S. Mhlanga, E. Nxumalo and B. Mamba, *J. Appl. Polym. Sci.* 2015, **DOI: 10.1002/app.41661**

Fouling control through the hydrophilic surface modification of poly(vinylidene fluoride) membranes
H. Jang, D.-H. Song, I.-C. Kim, and Y.-N. Kwon, *J. Appl. Polym. Sci.* 2015, **DOI: 10.1002/app.41712**

Hydroxyl functionalized PVDF-TiO_2 ultrafiltration membrane and its antifouling properties
Y. H. Teow, A. A. Latif, J. K. Lim, H. P. Ngang, L. Y. Susan and B. S. Ooi, *J. Appl. Polym. Sci.* 2015, **DOI: 10.1002/app.41844**

Enhancing the antifouling properties of polysulfone ultrafiltration membranes by the grafting of poly(ethylene glycol) derivatives via surface amidation reactions
H. Yu, Y. Cao, G. Kang, Z. Liu, W. Kuang, J. Liu and M. Zhou, *J. Appl. Polym. Sci.* 2015, **DOI: 10.1002/app.41870**

SEPARATION APPLICATIONS

Experiment and simulation of the simultaneous removal of organic and inorganic contaminants by micellar enhanced ultrafiltration with mixed micelles
A. D. Vibhandik, S. Pawar and K. V. Marathe, *J. Appl. Polym. Sci.* 2015, **DOI: 10.1002/app.41435**

Polymeric membrane modification using SPEEK and bentonite for ultrafiltration of dairy wastewater
A. Pagidi, Y. Lukka Thuyavan, G. Arthanareeswaran, A. F. Ismail, J. Jaafar and D. Paul, *J. Appl. Polym. Sci.* 2015, **DOI: 10.1002/app.41651**

Forensic analysis of degraded polypropylene hollow fibers utilized in microfiltration
X. Lu, P. Shah, S. Maruf, S. Ortiz, T. Hoffard and J. Pellegrino, *J. Appl. Polym. Sci.* 2015, **DOI: 10.1002/app.41553**

A surface-renewal model for constant flux cross-flow microfiltration
S. Jiang and S. G. Chatterjee, *J. Appl. Polym. Sci.* 2015, **DOI: 10.1002/app.41778**

Ultrafiltration of aquatic humic substances through magnetically responsive polysulfone membranes
N. A. Azmi, Q. H. Ng and S. C. Low, *J. Appl. Polym. Sci.* 2015, **DOI: 10.1002/app.41874**

BIOSEPARATIONS APPLICATIONS

Analysis of the effects of electrostatic interactions on protein transport through zwitterionic ultrafiltration membranes using protein charge ladders
M. Hadidi and A. L. Zydney, *J. Appl. Polym. Sci.* 2015, **DOI: 10.1002/app.41540**

Modification of microfiltration membranes by hydrogel impregnation for pDNA purification
P. H. Castilho, T. R. Correia, M. T. Pessoa de Amorim, I. C. Escobar, J. A. Queiroz, I. J. Correia and A. M. Morão, *J. Appl. Polym. Sci.* 2015, **DOI: 10.1002/app.41610**

Hemodialysis membrane surface chemistry as a barrier to lipopolysaccharide transfer
B. Madsen, D. W. Britt, C.-H. Ho, M. Henrie, C. Ford, E. Stroup, B. Maltby, D. Olmstead and M. Andersen, *J. Appl. Polym. Sci.* 2015, **DOI: 10.1002/app.41550**

Membrane adsorbers comprising grafted glycopolymers for targeted lectin binding
H. C. S. Chenette and S. M. Husson, *J. Appl. Polym. Sci.* 2015, **DOI: 10.1002/app.41437**

Journal of Applied Polymer Science

Development of functionalized doped carbon nanotube/polysulfone nanofiltration membranes for fouling control

Kholiswa Yokwana,[1] Nozipho Gumbi,[1] Feyisayo Adams,[2] Sabelo Mhlanga,[1] Edward Nxumalo,[1] Bheki Mamba[3]

[1]Department of Applied Chemistry, University of Johannesburg, Doornfontein 2028, South Africa
[2]Department of Petroleum Chemistry, School of Arts Sciences, American University of Nigeria, Yola Adamawa State, Nigeria
[3]Nanotechnology and Water Sustainability Research Unit, College of Engineering, Science and Technology, University of South Africa, Florida Campus, Johannesburg, South Africa
Correspondence to: B. Mamba (E-mail: bmamba@uj.ac.za)

ABSTRACT: This work describes the fabrication of nitrogen doped and phosphorus doped carbon nanotube (*f*P-CNT and *f*N-CNT)/polysulfone blend membranes via a phase inversion method. The structural morphology, hydrophilicity, rejection, and permeability properties of the blend membranes were found to be dependent on the amount and type of functionalized CNTs (*f*CNTs) incorporated (i.e., *f*N-CNTs, *f*P-CNTs). The results showed that PSf membranes modified with P- or N-doped CNTs have significantly improved hydrophilicity, thermal stability, water uptake, and surface charge compared to membranes modified with pristine *f*CNTs. Scanning electron microscopy studies demonstrated that the addition of the doped CNTs resulted in the formation of 'finger-like' structures subsequently leading to increased membrane porosities and pore sizes. Thus, doped CNTs imparted on the transport mechanism of the parent membranes resulting in enhanced flow rates and better selectivity. This increase could be due to a combination of steric limitations from the carboxylic functional groups present in their surfaces leading to electrostatic repulsions between functional groups present in the membranes and the humic acid molecules. © 2015 Wiley Periodicals, Inc. J. Appl. Polym. Sci. **2015**, *132*, 41835.

KEYWORDS: blends; composites; graphene and fullerenes; membranes; nanotubes; properties and characterization

Received 1 August 2014; accepted 25 November 2014
DOI: 10.1002/app.41835

INTRODUCTION

Membrane technology is used widely in the removal of different contaminants such as microorganisms and dissolved solids from water. Polysulfone (PSf) is a classical membrane material with excellent properties, and is broadly used in different fields such as water purification, biochemistry, gas separation, drugs extraction, etc.[1–3] However, PSf membranes suffer from high hydrophobicity, which causes them to be easily fouled resulting in reduced membrane efficiency i.e., flux decline and low rejection of contaminants (such as natural organic matter (NOM), heavy metals, salts, bacteria, and viruses). Fouling of PSf membranes further leads to shortened life span[4,5] and significantly hinders its application in water treatment. NOM has been identified as one of the major foulants for nanofiltration (NF) and forward osmosis (FO) membranes.[6] To date, much effort has been devoted on improving PSf membrane properties to enhance its performance in water treatment. For example, inorganic nanoparticles such as TiO_2, ZnO, SiO_2, and ZrO_2 have been used to modify PSf membranes to enhance its performance.[7–12]

Carbon nanotubes (CNTs), because of their unique mechanical, electrical, and electrochemical properties have stimulated an increasing interest in membrane technology. Although, CNTs are promising nanomaterials, they do have some limitations, which impart negatively on their use in polymer membrane synthesis. CNTs have poor dispersion and dissolution in different organic solvents, which cause difficulties during interaction with polymer matrices. Secondly, CNTs tend to agglomerate in membrane surfaces causing reduction in membrane performance.[13–15]

Several researchers have successfully fabricated blended polymeric membranes by incorporating CNTs resulting in new composite membranes with enhanced properties.[16,17] CNT/poly(methyl methacrylate) composite membranes with great mechanical and electrical properties and high thermal conductivity were prepared.[18] Choi *et al.*[19] demonstrated that CNT/PSf composite membranes are more hydrophilic than bare PSf membranes. Scanning electron microscopy (SEM) studies showed an increase in pore size of the blend membranes along

Additional Supporting Information may be found in the online version of this article.

with an increase in the content of CNTs up to 1.5%. In addition, PSf membranes modified with 4.0% content of CNTs were reported to have the best performance and more improved morphology. CNT/PSf blended membranes resulted in higher fluxes. However, lower protein rejections were observed for blended membranes compared to those of bare PSf membranes.[20,21]

In this work, we envisage that CNTs modified by means of doping with heteroatoms, such as boron, nitrogen, phosphorus, etc. will yield improved properties.[22,23] These modified CNTs can further improve the properties of polymer membranes. This is because doping can lead to highly efficient functionalization of the CNT surfaces compared to undoped CNTs, resulting in denser functionality and higher chemical reactivity with membrane backbones.[14,24,25]

This study thus focuses on developing novel doped CNT/PSf NF composite membranes with high permeability and selectivity and determining their performance with respect to humic acid fouling resistance in water treatment. Functionalized CNTs (*f*CNTs), *f*N-CNTs, and *f*P-CNTs were used as functional additives to modify PSf membranes thereby improving their performance in parameters such as the permeate flux decline and solute rejection. The *f*CNT/PSf nanocomposite membranes were characterized using SEM, Fourier transform infrared spectroscopy (FT-IR), thermal gravimetric analysis (TGA), Brunauer Emmett Teller (BET), contact angle analyzer, electrokinetic analyzer, and ultraviolet-visible absorption spectrometer (UV-Vis). A six cell cross-flow system was used to measure their permeability and to determine their antifouling efficiency and salt rejection.

EXPERIMENTAL

Materials

The materials used for membrane fabrication include PSf (obtained from Solvay Advanced Polymers - South Africa) and *N,N*-dimethylacetamide (DMAc) (Sigma-Aldrich); used as solvent to dissolve PSf polymer. Toluene, triphenylphosphine, nitric acid, acetonitrile (Merck), and ferrocene (purity $\geq$ 98%, B.D.H.) (Sigma-Aldrich) were used to synthesize the doped CNTs. Humic acid and sodium chloride (Sigma-Aldrich) were used to spike water as a foulant and electrolyte, respectively. Magnesium sulphate, also obtained from Sigma-Aldrich, was used without further purification. Deionized (DI) water was obtained from a water purification system (RO Process Ecopure G.I.C. Scientific) in the University of Johannesburg (Department of Applied chemistry).

CNT Synthesis and Functionalization

CNTs, N-CNTs, and P-CNTs were prepared using a floating catalyst chemical vapour deposition method and functionalized by a refluxing procedure to give *f*CNTs, *f*N-CNTs, and *f*P-CNTs.[26] Typically, the CNTs were refluxed in 55% nitric acid at 100°C for 4 h, followed by washing with DI water until a neutral pH (~7) was achieved. The resulting material was dried overnight in a vacuum oven at 100°C.

Membrane Preparation

The membranes were prepared via a phase inversion method.[21,27] In the preparation of pure PSf membranes, PSf was first dissolved in DMAc and stirred for 3 h at 80°C to form a homogenous mixture. The solution was then left overnight to eliminate air bubbles. The solution was hand cast onto a glass plate using a casting knife (Elcometer 3545 adjustable bird film applicator) set to 250 µm thickness. The cast film was exposed to ambient temperature for 10 s before it was immersed into a coagulated water bath at about 4°C for 30 min. The film was removed and dipped into a distilled water bath for 2 h followed by drying at room temperature. Membranes incorporating *f*CNTs, *f*N-CNTs, and *f*P-CNTs were fabricated in a similar fashion except that CNTs were first dispersed in DMAc by ultrasonication for 15 min to form a good dispersion. The different compositions of *f*CNT/PSf membranes are shown in Table I.

Table I. The Composition of Membrane Casting Solutions

Membrane type	PSf (wt %)	CNT content (wt %) *f* CNTs	*f*N-CNTs	*f*P-CNts	DMAc (wt %)
Pure PSf	15	-	-	-	85
0.1% *f*CNT/PSf	15	0.1			85
0.1% *f*N-CNT/PSf	15		0.1		85
0.1% *f*P-CNT/PSf	15			0.1	85
0.3% *f*CNT/PSf	15	0.3			85
0.3% *f*N-CNT/PSf	15		0.3		85
0.3% *f*P-CNT/PSf	15			0.3	85
0.5% *f*CNT/PSf	15	0.5			85
0.5% *f*N-CNT/PSf	15		0.5		85
0.5% *f*P-CNT/PSf	15			0.5	85

Membrane Characterization

The cross-section and surface morphology of the prepared membranes were investigated using a JEOL SEM. The samples were coated with gold to prevent electron charging. All images were acquired at 20 kV setting. Samples for cross-sectional images were first frozen in liquid nitrogen and then fractured and loaded onto the microscopy for analysis. Thermogravimetric analysis (Perkin Elmer TGA 4000 instrument) was used to determine the thermal stability of samples and the fraction of volatile components. A sample mass of approximately 10 mg was analyzed at the heating rate of 10°C/min in a temperature range of 30–800°C under oxygen atmosphere.

FT-IR spectroscopy was used for the determination of functional groups present in the membranes. FT-IR spectrometer (Perkin Elmer spectrum 100 instrument) with horizontal ATR device was used to characterize the prepared membranes. BET was used to determine the surface area, pore size, and pore volume of the samples. A sample mass of between 200 and 300 mg was degassed under nitrogen atmosphere and analyzed using liquid nitrogen.

The surface hydrophilicity of the prepared membranes was determined by measuring the contact angle using the sessile-drop method on a Data Physics Optical measuring instrument. The membrane samples were mounted on a planar glass plate.

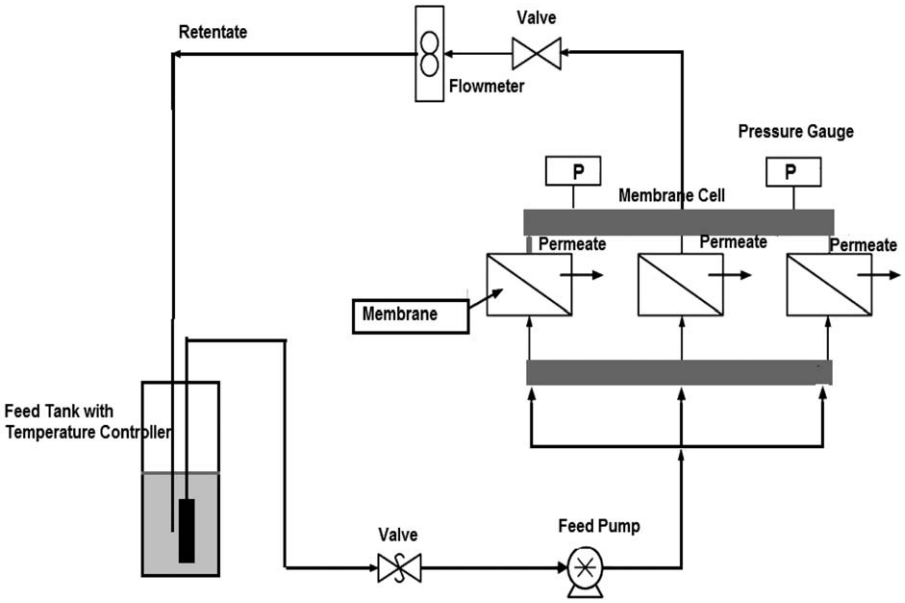

Figure 1. A schematic diagram of a cross-flow testing setup for membranes.

A total of 1 μL of DI water was carefully dropped on the top surface of the membrane from a syringe at a distance of about 0.5 cm using a syringe tip to avoid spreading of water drop. To minimize the experimental error, five drops of distilled water were placed randomly onto the surface of the membrane then the average contact angle measurements were reported. The surface charge and the zeta potential of the fabricated membrane were measured on a SurPASS Electrokinetic analyzer using a streaming potential analyzer (adjustably equipped) with a clamping gap cell of 20 × 10 mm for planar samples. Aqueous NaCl solutions at different pH (2–6) was used as electrolyte, pH was adjusted using HCl and NaOH solutions

Permeation Tests

Membrane Porosity. Membrane porosity was evaluated by first weighing a dry membrane and then soaking it in distilled water for 24 h, followed by drying the surface with a blotting paper. The wet membranes were completely dried by placing them in an oven at 80°C for 24 h and then weighing. The porosity of membranes (P) was calculated using eq. (1).

$$P(\%) = \left(\frac{W_w - W_d}{Ah}\right) \times 1000 \quad (1)$$

where, A is the membrane surface area (cm^2), h, the membrane thickness (mm), W_w, the weight of a wet membrane and W_d, is the weight of a dry membrane (g). To minimize the experimental errors, the membrane porosity was measured at least three times and average values were reported.

Water Uptake/Swelling Test. The membranes were immersed in distilled water at room temperature for 24 h. They were removed and blotted dry by a paper towel to remove the drops of water and weighed to get the mass of wet membranes. They were then dried at 80°C for 24 h in an oven and weighed again to get the mass of dry membranes. The water uptake was reported as weight percentage (water absorption) using the following equation.

$$\text{Water uptake}(\%) = \left(\frac{W_{wet} - W_{dry}}{W_{wet}}\right) \times 100 \quad (2)$$

Permeability and Fouling Test. A cross-flow membrane testing unit with an effective membrane area of 18.30 cm^2 was used for the permeation tests (Figure 1). The experiments were performed at a constant temperature of 22°C. The membranes were initially operated at a pressure of 100 psi for compaction using DI water overnight for stabilization; and then pressure was reduced to 50 psi and the pure water flux of the virgin membranes (J) was determined. The pure water flux was calculated using eq. (3).

$$J = \frac{V}{At} \quad (3)$$

V is the permeate volume (ℓ), A is the membrane effective area (m^2) and t is the time (h) necessary for the permeate volume to be collected.

The fouling behavior of the membranes was determined by the filtration of 100 mg/L HA aqueous solutions in 10 mM NaCl at a pH of 6.8. The rejection of $MgSO_4$and NaCl (pH 6.8) was also performed under the same conditions. Equation (4) was used to evaluate the membrane efficiency in removing salts from the feed solution.

$$R(\%) = \left[1 - \frac{C_p}{C_f}\right] \times 100 \quad (4)$$

C_f denotes concentration in the feed and C_p denotes concentration in the permeate (mg/L). The permeate flux decline (PFD) was used to determine the fouling extent of membranes. Permeate flux decline was calculated using the following equation.[28]

$$PFD(\%) = \left[1 - \frac{J}{J_o}\right] \times 100 \quad (5)$$

The concentrations of the feed and permeate solution were measured using an UV-Vis absorption spectroscopy (UV-2450

Table II. Water Contact Angles of PSf, *f*CNT/PSf, *f*N-CNT/PSf, and *f*P-CNT/PSf Composite Membrane Surfaces

	Contact angle (°)		
Content	*f*CNT/PSf	*f*N-CNT/PSf	*f*P-CNT/PSf
0.0%	68.7	68.7	68.7
0.1%	63.5	54.1	54.7
0.3%	60.5	50.4	52.8
0.5%	56.6	50.1	62.5

UV-Vis spectrophotometer (Shimadzu)) at a wavelength of 254 nm.

RESULTS AND DISCUSSION

FT-IR Spectroscopy Results

FT-IR spectroscopy peaks representing the symmetric O═S═O stretching vibrations were observed around 1294 and 1146 cm^{-1} in all membranes.[28] In addition, the stretches observed around 1280 cm^{-1} correspond to S—O stretch bands. The peak at 1236 cm^{-1} is characteristic of polysulfone membranes and can be attributed to the symmetric C—O—C stretching vibrations, whereas the peak found in the region 3090–2920 cm^{-1} corresponds to asymmetric stretch of the C—H band. The PSf membranes modified with undoped CNTs show similar patterns with pure PSf membrane. This suggests that the interaction between PSf and CNTs is poor as CNTs are inert. However, the spectra of blend membranes with *f*N-CNTs and *f*P-CNTs are different as C═O groups bonds are present (1738 cm^{-1}) formed by the addition of functionalized doped CNTs. This is a common observation when PSf membranes are modified by *f*CNTs.[21,29] The band in 1100–1350 cm^{-1} regions is characteristic of C—O single bond. The FT-IR spectra are shown in the Supporting Information (Figure S1).

Effect of *f*N-CNTs and *f*P-CNTs on the Hydrophilicity of PSf Membranes

Generally, membrane hydrophilicity depends on the values of water uptake and contact angle. The effect of water uptake on the hydrophilicity of the blended membranes is discussed in detail in the Effect of *f*CNTs on Water Uptake and Porosity of PSf Membranes section. Pure PSf membranes gave higher contact angles i.e., 68.7° (Table II). This is the highest contact angle value compared to the values of all the composite membranes (rendering the membranes less hydrophilic). *f*CNT/PSf membranes (0.1, 0.3, and 0.5 wt %) showed lower contact angles (versus PSf membrane contact angles) of 63.5, 60.5, and 56.6°, respectively, indicating that oxidised CNTs have a remarkable effect in transforming the PSf membrane surface hydrophilicity. As expected the hydrophilicity of the membranes was improved with the addition of *f*N-CNT as a result of —COOH, —OH, and —CO groups present on N-CNT in the *f*N-CNT/PSf composite membranes. In addition, water contact angles decreased with an increase in *f*CNT and *f*N-CNT loading in the membrane. Similar observations were made by Rahimpour *et al.*[30] after incorporating *f*CNTs into PES membranes. The improvement of hydrophilicity by the addition of *f*N-CNTs could reduce the interaction between the organic pollutants and the modified surface of the composite membranes leading to high water permeability and enhanced fouling resistance.[31,32]

On the other hand, modification of PSf with *f*P-CNTs (up to 0.3 wt % *f*P-CNTs) resulted in increased hydrophilicity indicating that *f*P-CNTs were capable of significantly enhancing the membrane surface hydrophilicity. However, the contact angle of *f*P-CNT/PSf membranes increased when 0.5 wt % of *f*P-CNTs was added (52.8–62.5°). This was a result of the presence of irregular structures and agglomeration in the membranes containing *f*P-CNTs, which further caused the membrane to be less hydrophilic.[33] However, this membrane is still more hydrophilic than the neat PSf membrane.

Effect of *f*CNTs on Water Uptake and Porosity of PSf Membranes

Pure PSf membranes were found to have low water uptake (30.5%), whereas *f*N-CNT/PSf membranes (highly hydrophilic membranes) had significantly high water uptake potentials (Table III). The water uptake abilities of the *f*N-CNT/PSf membranes increased with an increase in the concentration of *f*N-CNTs. This is attributed to the increase in carboxylic acid groups and the presence of N heteroatoms on the CNTs, which further caused the surface to be more reactive resulting in enhanced porosity. This led to increased water absorption at increased concentration of functionalized doped CNTs. This behavior is attributed to enhanced macro-void formation, which favors high surface area for water uptake inside the membrane.

In addition, the porosity of PSf membranes modified with *f*N-CNTs and *f*P-CNTs increased with an increase in the amount of CNTs added to the membrane structure. However, a further increase in doped CNTs to 0.5 wt % resulted in decreased porosity (Table III). This unusual behavior could be related to the agglomeration of functionalized doped CNTs at high % thereby causing blockage of the pores on the surface of the composite membranes due to delayed phase separation and increased viscosity.[34] The same trends for porosity and water uptake were observed for *f*P-CNT/PSf membranes. The addition of *f*P-CNTs up to 0.3 wt % improved the water uptake (from

Table III. Porosity and Water Content for Different Membranes

Membrane type	Percentage water absorption (%)	Porosity (%)
PSf	30.5	5.9
0.1% *f*CNT/PSf	30.1	13.2
0.1% *f*N-CNT/PSf	32.6	4.7
0.1% *f*P-CNT/PSf	35.6	6.4
0.3% *f*CNT/PSf	27.3	5.3
0.3% *f*N-CNT/PSf	63.8	26.1
0.3% *f*P-CNT/PSf	37.3	7.3
0.5% *f*CNT/PSf	39.9	8.1
0.5% *f*N-CNT/PSf	34.0	6.3
0.5% *f*P-CNT/PSf	23.9	4.0

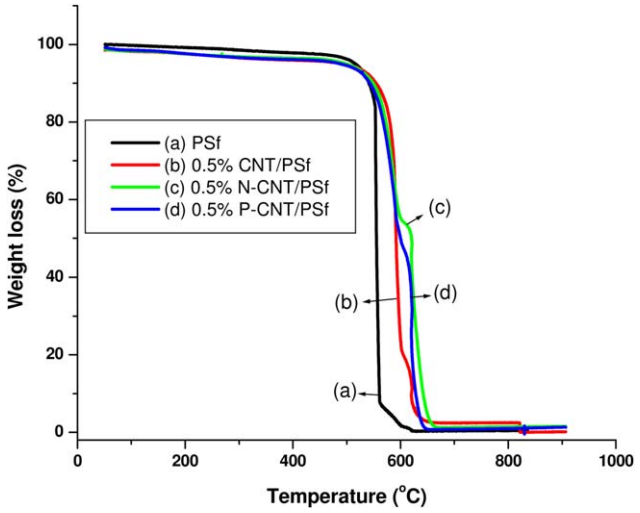

Figure 2. TGA curves of PSf, *f*CNT/PSf, *f*N-CNT/PSf, and *f*P-CNT/PSf composite membranes. [Color figure can be viewed in the online issue, which is available at wileyonlinelibrary.com.]

30.5 to 37.3%) and porosity (from 5.9 to 7.3%) of PSf membranes.

Effects of *f*N-CNTs and *f*P-CNTs on the Thermal Stability of PSf Membranes

The thermal stability of different types of NF composite membranes were measured by TGA under air. The decomposition of pure PSf membranes occurred at about 549.7°C as shown in Figure 2. However, when *f*CNTs, *f*N-CNTs, or *f*P-CNTs were incorporated into the PSf matrix, the decomposition shifts to higher temperatures. This indicates that composite membranes have improved thermal stability compared to pure PSf membrane due to the inclusion of the highly thermally stable carbon material.[35]

In addition, the decomposition temperature of *f*CNT/PSf composite membranes decreased from 590 to 570°C as the amount of *f*CNTs added into the PSf membrane increased from 0 to 0.5%. This can be attributed to the poor dispersion of CNTs in the PSf matrix. However, in the case of *f*N-CNT/PSf membranes thermal stability increased with an increase in the content of *f*N-CNTs added into the membranes. A higher decomposition temperature of about 615°C was noted in the case of 0.5% *f*N-CNT/PSf composite membranes. This confirms that the *f*N-CNT/PSf composite membranes have improved thermal stability than pure PSf and their *f*P-CNT counterparts. The improvement in thermal stability is due to the homogeneous dispersion of *f*N-CNTs into the PSf membrane, as a result of the existence of strong interactions between the —COOH groups on *f*N-CNT outer surfaces and —SO_2 groups of PSf. These interactions are further due to strong hydrogen bonds between the *f*N-CNTs and the PSf polymer matrix thus modifying the structure of the polymer network. All other TGA data for the composite membranes are presented in Figure S2 (Supporting Information).

Membrane Microstructure

To understand the influence of doped CNT on the membrane structure, SEM cross-section and surface morphology studies were performed (Figures 3 and 4). The PSf membranes without CNTs exhibit a typical asymmetric structure, smooth surface, and macro-voids structures. As expected, the surface morphology of a 0.3% CNT/PSf composite membrane had a

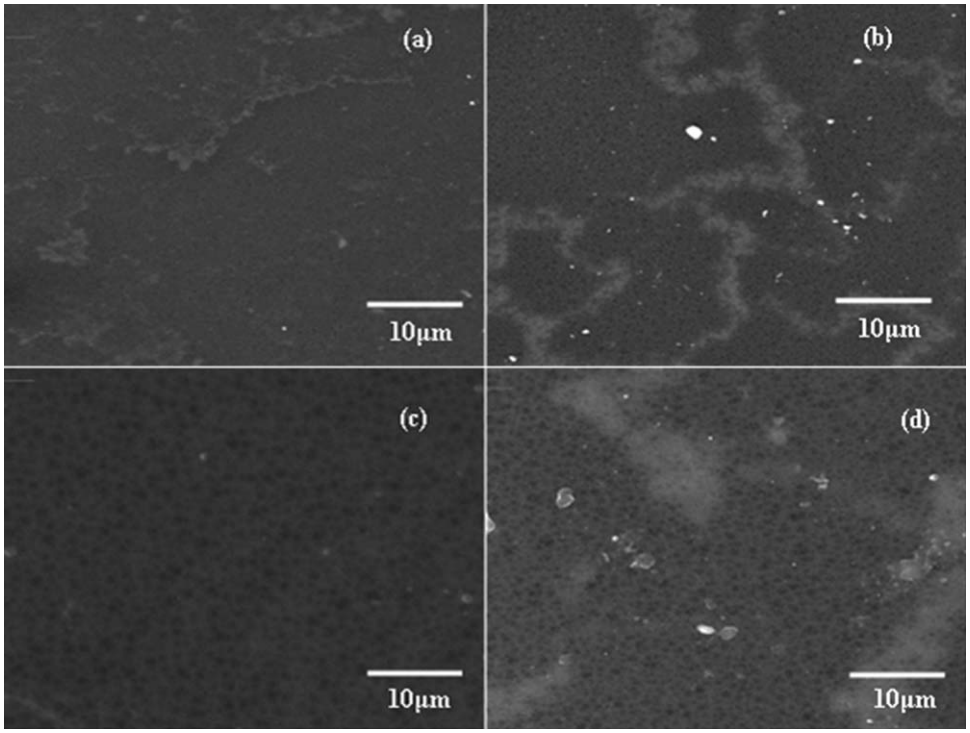

Figure 3. SEM images of (a) PSf membranes (b) 0.3% *f*CNT/PSf membranes (c) 0.3% *f*N-CNT/PSf membranes, and (d) 0.3% *f*P-CNT/PSf membranes.

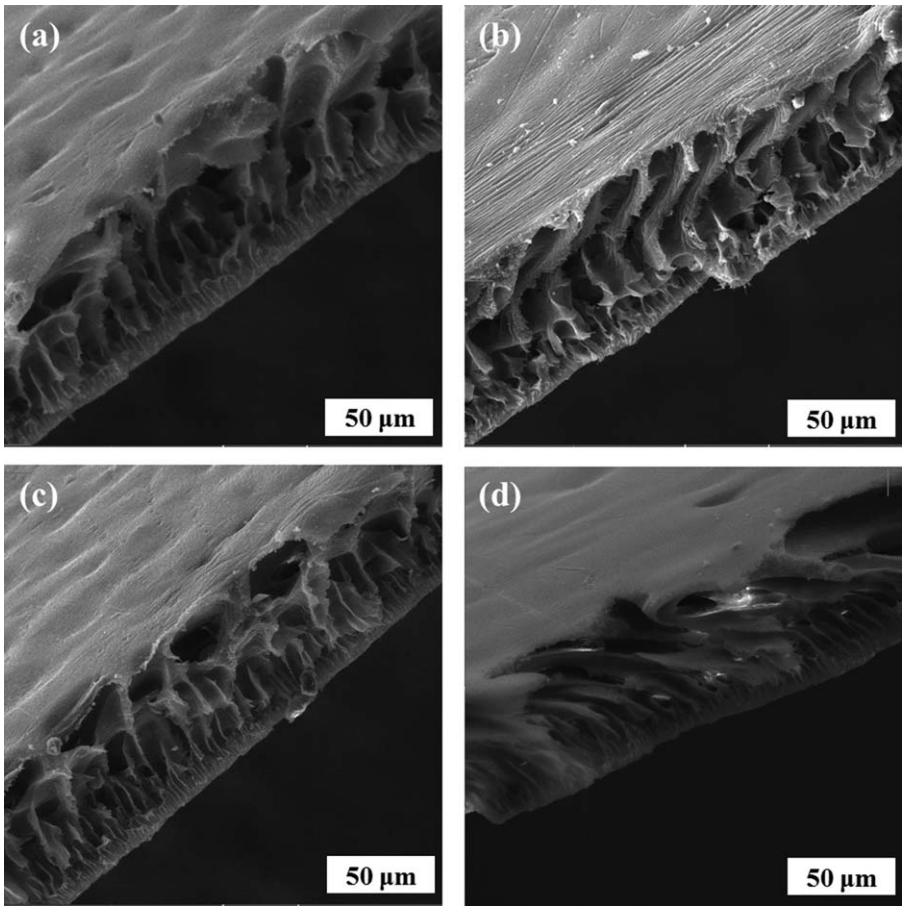

Figure 4. Cross-section SEM images of (a) PSf membranes (b) 0.3% *f*CNT/PSf membranes (c) 0.3% *f*N-CNT/PSf membranes, and (d) 0.3% *f*P-CNT/PSf membranes.

nonuniform morphology [Figure 3(b)], whereas PSf modified with 0.3% of *f*N-CNTs and *f*P-CNTs showed uniform surfaces [Figure 3(c,d)]. Indeed, the formation of porous macropores and finger-like micro-void structures was suppressed by the addition of CNTs in the membrane structure [Figures 3(b) and 4(b)]. In addition, there was a significant increase in the density of pores and fully developed macro-void pores when PSf membranes were modified with 0.3% *f*N-CNTs [Figures 3(c) and 4(c)]. However, with further increase in *f*N-CNT content, a slight decrease in the density of pores below the separation layer

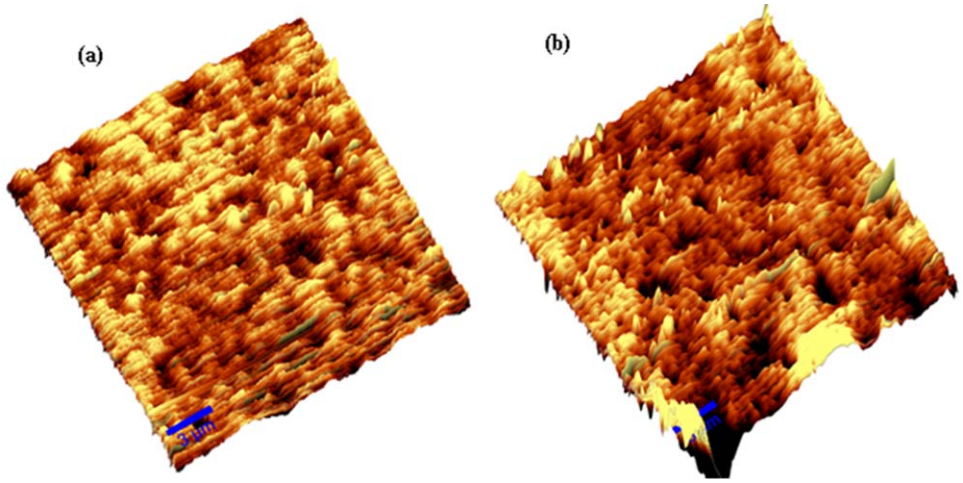

Figure 5. AFM images for the outer surface of composite membranes: (a) 0.3% *f*N-CNT/PSf and (b) 0.3% *f*P-CNT/PSf. [Color figure can be viewed in the online issue, which is available at wileyonlinelibrary.com.]

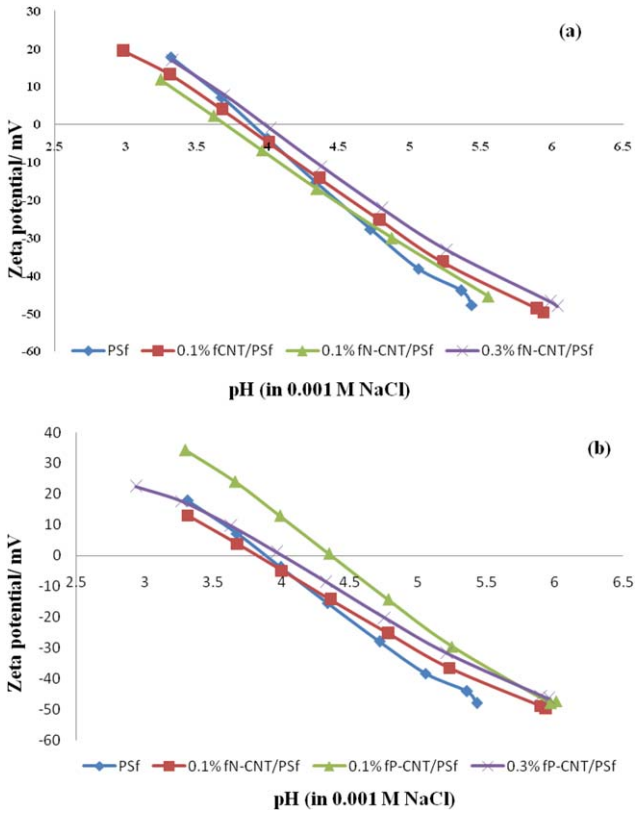

Figure 6. The zeta potential as a function of pH for unused membranes (a) PSf, 0.1% *f*CNT/PSf, 0.1% *f*N-CNT/PSf, and 0.3% *f*N-CNT/PSf (b) PSf, 0.1% *f*P-CNT/PSf and 0.3% *f*P-CNT/PSf. Background electrolyte: 0.001*M* NaCl. [Color figure can be viewed in the online issue, which is available at wileyonlinelibrary.com.]

was observed. This observation is in agreement with the result obtained from the porosity studies (Table III). Clearly, the formation of membrane pore sizes and porosity depended on the time taken for phase separation to begin. The faster the phase separation, the larger the pores, whereas, a delay in time for separation results in thick, smaller pore sizes, and less porous surfaces. The increase in pore sizes/densities might be explained by the increasing amount of functionalized doped CNTs in the casting solution to 0.3 wt %, resulting in enhanced phase separation[21,29] whereas, a further increase in *f*N-CNTs led to a delay in phase separation.

SEM investigations thus demonstrate that 0.3% *f*P-CNT/PSf membranes have more porous surfaces than CNT/PSf membrane (but fewer pores compared to *f*N-CNT/PSf composite membranes, which have larger pores and finger-like structures). Further, circle-shape patterns were observed on the sub-layers of the *f*P-CNT/PSf composite membranes. This therefore indicates that the *f*N-CNTs were homogenously dispersed on the membrane polymer matrix due to increased solubility of *f*N-CNTs in the casting solvent during the phase inversion process.

Atomic Force Microscopy

Figure 5 shows 3D AFM surface morphology images of 0.3% *f*N-CNT/PSf and 0.3% *f*P-CNT/PSf NF blended membranes at a scan area of 3 μm. The bright high peaks represent the highest points on the surface of the membrane, whereas the dark depressions represent pores. Figure 6 clearly shows significant differences in morphology of PSf membranes modified with different functionalized doped CNTs (*f*P-CNTs and *f*N-CNT). Figure 5(a) show that PSf membranes modified with 0.3 wt % *f*N-CNTs have less surface roughness, whereas *f*P-CNT/PSf membranes have high surface roughness [Figure 5(b)]. *f*N-CNTs thus produce composite membrane with smoother surfaces compared to the *f*P-CNT/PSf composite membrane. This confirms that there was an increase in hydrophilicity of the *f*N-CNT/PSf membrane (Table II). The enhancement in the degree of hydrophilicity and surface roughness of the membrane is known to result in lower fouling surfaces.[10] Similar observations were made with all other doped CNT/PSf membranes and our previous work performed thorough investigations on this subject (thus, all the other AFM images were not presented in this work).[27,36]

Surface Charge of CNT/PSf Composite Membranes

Figure 6 illustrates the zeta potential as a function of pH determined using NaCl as an electrolyte. The results obtained are however not remarkably different. This may be understood when considering the possibility that the CNTs get coated by a thin PSf layer during the manufacturing process. Nevertheless, it was found that *f*N-CNT/PSf composite surface charge were different to PSf modified with *f*P-CNTs and *f*CNTs composite membranes.

The membrane surface charge contributes to the improvement of HA absorption on the composite membranes due to the electrical conductivity of functionalized doped CNTs as a result of the functional groups present in the membrane surface. The modification of PSf with (*f*N-CNTs or *f*P-CNTs) resulted in a conductive membrane material. This may be due to increased pore size (ionic conductance) or due to the electric conductance of CNTs. With the membranes modified with 0.1 wt % *f*N-CNTs and 0.1 wt % *f*P-CNTs, no conductance could be detected; however, when 0.3 wt % *f*N-CNTs or 0.3 wt % *f*P-CNTs were incorporated to the PSf matrix, a significant contribution to interfacial conductance was observed.

PSf membranes with 0.1 wt % *f*N-CNTs show an isoelectric point (IEP), which is shifted to lower pH values. At pH values lower than those of the IEP of the membrane, the membrane surface had positive charges due to proton adsorption, whereas at a pH values higher than the IEP of the membrane, it has negatively charged values due to proton desorption and hydroxyl anion adsorption. Although PSf membranes blended with 0.1 wt % *f*P-CNTs show an IEP, which is shifted to higher pH, the composite PSf membrane with 0.1 wt % *f*CNT showed no significant difference from the bare PSf membrane. The composite membranes zeta potential decreased as the pH increased and at higher pH values a more negative zeta potential was observed (Figure 6). In addition, the PSf modified with 0.3 wt % *f*N-CNTs or *f*P-CNTs does not appear to have significantly different zeta potentials. However, it was observed that increase in concentration of *f*N-CNTs or *f*P-CNTs in the membrane blends resulted in high negative charges at pH 5–6.

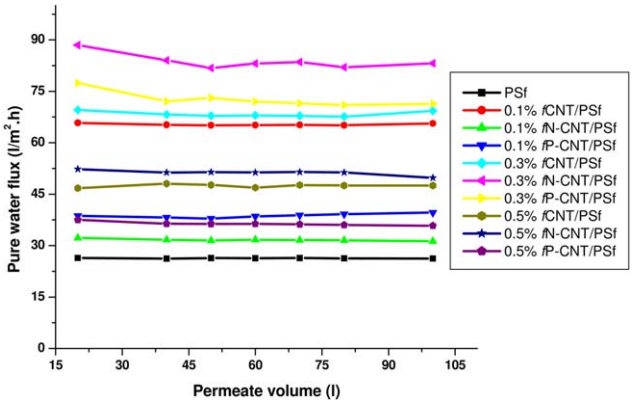

Figure 7. Pure water flux patterns of PSf membranes containing different concentrations of *f*CNTs, *f*N-CNTs, and *f*P-CNTs. [Color figure can be viewed in the online issue, which is available at wileyonlinelibrary.com.]

The higher negative charge of the doped CNT/PSf composite membrane surface is attributed to the presence of —COOH groups on their surfaces. The increase is further due to the adsorption of anions such as Cl^- and OH^- from solution to cause a more negative zeta potential. Membranes with negative zeta potential values exhibited more hydrophilic surfaces and high water uptake as shown Table II.

The negatively charged surfaces of composite membrane further result in more enhanced salt rejection and antifouling resistance, due to electrostatic repulsion between the HA molecules and membrane surfaces, which further contributes to the decreased HA adsorption on the modified membranes. The charge of the membrane is significant to membrane performance because charge affects the electrostatic repulsion between the ions and the charged molecules with membrane surface charge. Moreover, because of membrane functional groups, the adsorbed OH^- and Cl^- surfactant molecules in the membrane surface provide an additional filtration layer that could result in enhanced salt rejection. This can be explained by the ion charge; if salt ions have the same charge as those of the composite membranes, repulsion between the salt and the membrane surface could occur thus causing salt ions to diffuse back to the solution resulting in higher salt rejections. This is further discussed in the Effect of CNTs on the Salt Rejection Capabilities of Membranes section.

Membrane Permeability Studies

As shown in Figure 7, differences in permeability were obtained in the different membranes. This is due to different properties such as pore size, porosity, and surface hydrophilicity for the membranes. The permeability increased with an increase in CNT content (up to 0.3%). In addition, the permeability of 0.3% *f*CNT/PSf composite membranes was lower than that of *f*N-CNT/PSf and *f*P-CNT/PSf composite membranes. When 0.5 wt % of CNTs were loaded, the permeability decreased due to the decrease in pore size and porosity (see the Effect of *f*CNTs on Water Uptake and Porosity of PSf Membranes section).

The bare PSf membranes had the lowest flux (26 L/m^{2}h) due to its low hydrophilicity. A maximum flux of about 85 L/m^{2}h was obtained when 0.3% *f*N-CNTs were used and this decreased when greater amounts of CNTs were added into the PSf membrane.[16,17] In general, the fluxes for all the composite membranes containing CNTs were larger than those of bare PSf membrane. Consequently, the increase in *f*CNTs, *f*N-CNTs, and *f*P-CNTs mass ratio into PSf membrane led to the formation of less porous membranes, which led to flux decline.

Membrane Antifouling Properties

Figure 8 represent the flux decline behavior as a function of operation time for 100 mg/L HA spiked with 10 m*M* NaCl solution at a pressure of 50 psi. A sharp drop in water flux was observed within the first 2 h for bare PSf, 0.1% *f*CNT/PSf, *f*N-CNT/PSf, *f*P-CNT/PSf, and 0.3% *f*CNT/PSf composite membranes. This could be due to the decrease in pore restriction and the initial deposition of the HA colloids on the membrane surface. The adsorption of HA molecule on the membrane surface evidently hindered the diffusion of water molecules. As a result, a decrease in the net driving force for water transport across the membrane to water flux decline. A stable flux for all membranes was obtained after a period of 15 h.

This work thus shows that fouling resistance is enhanced by N-CNTs incorporation into the membranes. The 0.3 and 0.5% *f*N-CNT/PSf and 0.3% *f*P-CNT/PSf composite membranes exhibited lower flux decline of about 85%. This observation is analogous to the increase in membrane hydrophilicity and high negatively charged surface (Table II and Figure 6). The hydrophilic surface repels the relatively hydrophilic HA molecules and subsequently reduce HA adsorption and enhance membrane fouling. In addition, this suggested that the adsorption of HA on the blended membranes was weaker than that between HA and bare PSf membrane. Indeed, the composite membranes had higher fluxes and less fouling propensity. However, an increase in *f*P-CNTs addition up to 0.5 wt % into the composite membranes led to high flux decline due to the agglomeration of *f*P-CNTs in the polymer matrix of the composite membranes as discussed in previous sections.

This is expected, because it is now known that hydrophobic membranes are fouled more easily than hydrophilic membranes

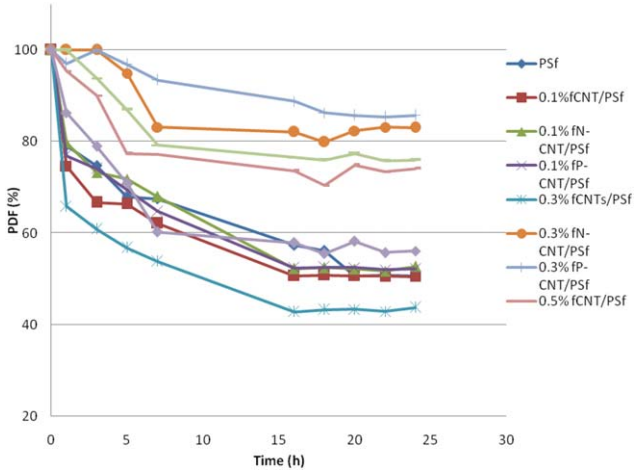

Figure 8. PFD patterns of PSf and composite membranes with different CNT content. [Color figure can be viewed in the online issue, which is available at wileyonlinelibrary.com.]

Table IV. Water Flux and Rejection Data of NaCl and $MgSO_4$ (10 m*M*) on Pure PSf and Different Composite Membranes

Membrane type	Water flux (L/m^{2}h)	NaCl rejection (%)	$MgSO_4$ rejection (%)
Pure PSf	26.3	30.1	88.1
0.1% *f*CNT/PSf	65.3	28.5	86.5
0.1% *f*N-CNT/PSf	31.7	29.1	88.0
0.1% *f*P-CNT/PSf	38.7	30.1	90.0
0.3% *f*CNT/PSf	68.3	30.0	90.8
0.3% *f*N-CNT/PSf	84.7	31.6	92.6
0.3% *f*P-CNT/PSf	72.6	32.3	93.3
0.5% *f*CNT/PSf	47.5	29.8	90.8
0.5% *f*N-CNT/PSf	51.3	33.5	95.0
0.5% *f*P-CNT/PSf	36.4	31.7	92.8

due to hydrophobic–hydrophobic interaction between solute and membrane surface.[37] In addition, membrane fouling is governed by the interplay between chemical and physical (hydrodynamic) interactions.[38,39] The maximum antifouling improvement of more than 80% was obtained for *f*N-CNT/PSf NF composite membranes. The modification of the PSf membranes by doped CNTs improved the surface charge, pore control, and cake-enhanced polarization concentration of the membrane through fouling. Thus, an improvement in surface charge, hydrophilicity, less surface roughness, and porosity led to improved membrane fouling resistance.

Effect of CNTs on the Salt Rejection Capabilities of Membranes

The salt rejection for both NaCl and $MgSO_4$was measured using a conductivity meter. To evaluate the filtration efficiency in removing salts from the feed solution, we used eq. (4). Table IV shows that NaCl rejection of *f*CNT/PSf blend membranes increased from 28.5 to 30.0% and from 86.5 to 90.8 for $MgSO_4$. A further increase in the amount of *f*CNTs (to 0.5%) resulted in a decrease in the salt rejection (30.0–29.8% for NaCl and 90.8–89.0 for $MgSO_4$). On the other hand, the flux dropped drastically from 68.3 to 47.5 L/m^{2}h. The addition of *f*N-CNTs to the membrane resulted in an increase in salt rejection [from 29.1 to 33.5% (NaCl)] and from 88.0 to 95.0% (MgSO4) also accompanied by a decrease in water flux from 84.7 to 51.3 L/m^{2}h, respectively (Table IV). This observation is similar to the result reported by Qui *et al.*[20] and Shawky *et al.*[40] where PSf and PA were modified with *f*CNTs and the resulting composite membranes demonstrated an increase in salt rejection accompanied by a decrease in both permeability and water flux.

The blending of PSf with *f*N-CNTs resulted in strong interactions between the CNTs and PSf matrix forming a compact structure.[31,32,41] The compatibility of the network structure increased with an increase in the amount of doped CNTs and undoped CNTs in the composite membrane. Thus, the lower water flux and higher salt rejection of $MgSO_4$was attributed to the network structure.[19–21,42,43] In the case of modification with *f*P-CNTs, the rejection of both salts increased as the concentration of *f*P-CNTs increased up to 0.3 wt % in the composite membranes. The differences in solute rejections are in accordance with the increased hydrophilicity and porosity as a result of increased air gap length.[35,44] All the modified membranes were found to reject about 32% of NaCl (lower) and about 82% of $MgSO_4$ (higher). This is consistent with the significant enhancement in membrane pore size, roughness, surface charge, and hydrophilicity properties. In addition, membranes with smaller pore sizes prevented solutes from penetrating the pores and thus reducing the possibility of pore blockage.

CONCLUSION

PSf membranes incorporated with *f*N-CNTs and *f*P-CNTs were successfully fabricated via a modified phase inversion process. Highly negatively charged surfaces, high surface areas, pore sizes, and wider 'finger-like' pore structures were found on the internal structure of the NF composite membranes. Water flux and salt rejection increased significantly indicating that an increase in pore size and macro-voids led to enhanced passage mechanisms resulting from the addition of CNTs on the matrix (due to improved hydrophilicity). This is because the CNTs incorporated into the membranes have heteroatoms (which necessitated active site and defects formation in the tubes), which subsequently led to an increased degree of chemical functionalization (—COOH, —CO). This in turn helped increase the finger-like structures and increased membrane pore sizes/densities, hydrophilicity, and chemical reactivity, thus, impacting positively on their performance. Moreover fouling was improved by about 30% when low fractions of *f*N-CNT or *f*P-CNTs were added into the PSf matrix. Thus, the morphology, hydrophilicity, rejection, and permeability properties of the blend membranes were found to be dependent on the amount and type of *f*CNTs incorporated.

ACKNOWLEDGMENTS

This research work was performed in the Department of Applied Chemistry, University of Johannesburg (South Africa). The authors gratefully acknowledge the Department of Science/Mintek Nanotechnology Innovation Centre for financial support.

REFERENCES

1. Brunet, L.; Lyon, D. Y.; Zodrow, K.; Rouch, J.-C.; Caussat, B.; Serp, P.; Remigy, J.-C.; Wiesner, M. R.; Alvarez, P. J. J. *Environ. Eng. Sci.* **2008**, *25*, 565.
2. Sotto, A.; Boromand, A.; Balta, S.; Kim, J.; Van der Bruggen, B. *J. Mater. Chem.* **2011**, *21*, 10311.
3. Armstrong, S. R.; Offord, G. T.; Paul, D. R.; Freeman, B. D.; Hiltner, A.; Baer, E. *J. Appl. Polym. Sci.* **2014**, *131*, 39765.
4. Shen, Y.; Zhao, W.; Xiao, K.; Huang, X. *J. Membr. Sci.* **2010**, *346*, 187.
5. Shon, H. K.; Vigneswaran, S.; Kim, I. S.; Cho, J.; Ngo, H. H. *J. Membr. Sci.* **2006**, *278*, 232.
6. Tang, C. Y.; Kwon, Y. N.; Leckie, J. O. *J. Membr. Sci.* **2007**, *290*, 86.

7. Taurozzi, J. S.; Arul, H.; Bosak, V. Z.; Burban, A. F.; Voice, T. C.; Bruening, M. L.; Tarabara, V. V. *J. Membr. Sci.* **2008**, *325*, 58.
8. Leo, C. P.; Cathie Lee, W. P.; Ahmad, A. L.; Mohammad, A. W. *Sep. Purif. Technol.* **2012**, *89*, 51.
9. Aerts, P.; Kuypers, S.; Genné, I.; Leysen, R.; Mewis, J.; Vankelecom, I. F. J.; Jacobs, P. A. *J. Phys. Chem.* **2006**, *110*, 7425.
10. Hamid, N. A. A.; Ismail, A. F.; Matsuura, T.; Zularisam, A. W.; Lau, W. J.; Yuliwati, E.; Abdullah, M. S. *Desalination* **2011**, *273*, 85.
11. Ahamed, A. L.; Majid, M. A.; Ooi, B. S. *Desalination* **2011**, *268*, 266.
12. Li, J.-B.; Zhu, J.-W.; Zheng, M.-S. *J. Appl. Polym. Sci.* **2007**, *103*, 3623.
13. Rahmat, M.; Hubert, P. *Compos. Sci. Technol.* **2011**, *72*, 72.
14. Hirsch, A.; Vostrowsky, O. *Chem. Mater. Sci.* **2005**, *245*, 193.
15. Kong, H.; Gao, C.; Yan, D. *J. Am. Chem. Soc.* **2004**, *126*, 412.
16. Jiang, Z.; Hornsby, P.; McCool, R.; Murphy, A. *J. Appl. Polym. Sci.* **2012**, *123*, 2676.
17. Singh, B. K.; Kar, P.; Shrivastava, N. K.; Banerjee, S.; Khatua, B. B. *J. Appl. Polym. Sci.* **2012**, *124*, 3165.
18. Lahelin, M.; Vesterinen, A.; Nykänen, A.; Ruokolainen, J.; Seppälä, J. *Eur. Polym. J.* **2011**, *47*, 873.
19. Choi, J.-H.; Jegal, J.; Kim, W.-N. *J. Membr. Sci.* **2006**, *284*, 406.
20. Qui, S.; Wu, L.; Pan, X.; Zhang, L.; Chen, H.; Gao, C. *J. Membr. Sci.* **2009**, *342*, 165.
21. Celik, E.; Park, H.; Choi, H.; Choi, H. *Water Res.* **2011**, *45*, 274.
22. Nxumalo, E. N.; Coville, N. J. *Materials* **2010**, *3*, 2141.
23. Glerup, M.; Krstic, V.; Ewels, C. P.; Holzinger, M.; Van Lier, G. In Doped Nanomaterials and Nanodevices, Wei, C., Ed.; American Scientific Publishers, **2008**.
24. Golberg, D.; Dorozhkin, P. S.; Bando, Y.; Dong, Z.-C.; Tang, C. C.; Uemura, Y.; Grobert, N.; Reyes-Reyes, M.; Terrones, H.; Terrones, M. *Appl. Phys. A* **2003**, *76*, 499.
25. Xiao, K.; Liu, Y.; Hu, P.; Yu, G.; Sun, Y.; Zhu, D. *J. Am. Chem. Soc.* **2005**, *127*, 8614.
26. Nxumalo, E. N.; Letsoala, P. J.; Cele, L. M.; Coville, N. J. *J. Organomet. Chem.* **2010**, *695*, 2596.
27. Adams, F. V.; Nxumalo, E. N.; Krause, R. W. M.; Hoek, E. M. V.; Mamba, B. B. *J. Membr. Sci.* **2012**, *405*, 291.
28. Balta, S.; Sotto, A.; Luis, P.; Benea, L.; Van der Bruggen, B.; Kim, J. *J. Membr. Sci.* **2012**, *389*, 155.
29. Nechifor, G.; Voicu, S. I.; Nechifor, A. C.; Garea, S. *Desalination* **2009**, *241*, 342.
30. Rahimpour, A.; Jahanshahi, M.; Khalili, S.; Mollahosseini, A.; Zirepour, A.; Rajaeian, B. *Desalination* **2012**, *286*, 99.
31. Yang, Y.; Wang, P.; Zheng, Q. *J. Polym. Sci. Part B: Polym. Phys.* **2006**, *44*, 879.
32. Song, R.; Yang, D.; He, L. *J. Mater. Sci.* **2008**, *43*, 1205.
33. Ballinas, L.; Torras, C.; Fierro, V.; Garcia-Valls, R. *J. Phys. Chem. Solids.* **2004**, *65*, 633.
34. Ma, P.-C.; Siddiqui, N. A.; Marom, G.; Kim, J.-K. *Compos. Part A-Appl. Sci.* **2010**, *41*, 1345.
35. Yang, J.; Wang, X.; Wang, X.; Jia, R.; Huang, J. *J. Phys. Chem. Solids* **2010**, *71*, 448.
36. Phao, N.; Nxumalo, E. N.; Mamba, B. B.; Mhlanga, S. D. *Phys. Chem. Earth Parts A/B/C* **2013**, *66*, 148.
37. Yu, H.-Y.; Hu, M.-X.; Xu, Z.-K.; Wang, J.-L.; Wang, S.-Y. *Sep. Purif. Technol.* **2005**, *45*, 8.
38. Hong, S.; Elimelech, M. *J. Membr. Sci.* **1997**, *132*, 159.
39. Seidel, A.; Elimelech, M. *J. Membr. Sci.* **2002**, *203*, 245.
40. Shawky, H. A.; Chae, S. -R.; Lin, S.; Wiesner, M. R. *Desalination* **2011**, *272*, 46.
41. Li, W.; Chen, X.; Chen, C.; Xu, L.; Yang, Z.; Wang, Y. *Polym. Compos.* **2008**, *29*, 972.
42. Lee, S. Y.; Kim, H. J.; Patel, R.; Im, S. J.; Kim, J. H.; Min, B. R. *Polym. Adv. Technol.* **2007**, *18*, 562.
43. Kim, C. K.; Kim, J. H.; Roh, I. J.; Kim, J. J. *J. Membr. Sci.* **2000**, *165*, 189.
44. Xu, P.; Drewes, J. E.; Kim, T. U.; Bellona, C.; Amy, D. J. *Membr. Sci.* **2006**, *279*, 165.